

Mineral Processing and Extractive Metallurgy Review

An International Journal

ISSN: (Print) (Online) Journal homepage: <https://www.tandfonline.com/loi/gmpr20>

Transport Phenomena in Copper Bath Smelting and Converting Processes – A Review of Experimental and Modeling Studies

Kezhou Song & Ari Jokilaakso

To cite this article: Kezhou Song & Ari Jokilaakso (2020): Transport Phenomena in Copper Bath Smelting and Converting Processes – A Review of Experimental and Modeling Studies, Mineral Processing and Extractive Metallurgy Review, DOI: [10.1080/08827508.2020.1806835](https://doi.org/10.1080/08827508.2020.1806835)

To link to this article: <https://doi.org/10.1080/08827508.2020.1806835>



© 2020 The Author(s). Published with license by Taylor & Francis Group, LLC.



Published online: 10 Sep 2020.



Submit your article to this journal [↗](#)



Article views: 125




View related articles [↗](#)



View Crossmark data [↗](#)

Transport Phenomena in Copper Bath Smelting and Converting Processes – A Review of Experimental and Modeling Studies

Kezhou Song and Ari Jokilaakso 

School of Chemical Engineering, Department of Chemical and Metallurgical Engineering, Aalto University, Espoo, Finland

ABSTRACT

Bath smelting and converting technologies for copper production have been improved, resulting in higher production efficiency and less polluting emissions. Reported studies on experimental and computational modeling approaches are reviewed in this paper, focusing on adjustable variables and flow details, for a thorough understanding of the complex flow phenomena of the high-temperature reactors used. Results from water models and Computational Fluid Dynamics (CFD) simulations indicate that the transport phenomena in different reactors should be analyzed separately, as flow behavior exhibits significant differences in different gas injecting regimes and furnace structures. Mixing behavior and further optimization for most furnaces are presented in this review, showing a considerable degree of agreement between experiments and computational simulations. In general, a deeper nozzle or tuyere level with a higher gas flow rate are factors in the majority of copper bath smelting and converting cases. However, the dynamic parameters cannot be infinitely increased, but should be maintained within an appropriate range to provide relatively high mixing efficiency while preventing refractory corrosion due to splashing. Research on detailed flow phenomena including bubbles and surface waves is relatively scarce. It is suggested that the most efficient reaction areas for furnaces in jetting and bubbling regimes are totally different, due to the differences in bubble behavior. Concerning the bath surface, the behavior of transversal standing waves and longitudinal waves has been preliminarily revealed using water models, suggesting that standing waves tend to disappear in particular ranges of bath height and gas flow rate.

KEYWORDS

Flow phenomena; water model; CFD; mixing efficiency; copper bath smelting; copper bath converting; bubble behavior; surface wave

1. Introduction

In the past 50 years, the consumption of copper and copper alloys has gradually increased due to expanding demand from infrastructure construction, industrial equipment production, and electronic technologies, as a robust growth of the market in developing countries (International Copper Study Group 2019; Newcomb 1985). In 2018, production of refined copper reached a value 5 times that of its value in 1960, and the secondary-refined output accounted for nearly 20% of the total, showing a slowly increasing trend (International Copper Study Group 2019). Modern copper matte smelting includes flash smelting furnaces (FSF) and bath smelting furnaces. Outotec flash smelting (FS) technologies have been widely adopted in copper production and account for 43% of the total copper smelting capacity (Wang et al. 2019). In FS processes, concentrate powder, flux, and enriched oxygen are mixed in a suspension stage and react very fast (Kojo, Jokilaakso and Hanniala 2000), giving significant advantages in industrial practice, leading to a large amount of research work (Guntoro et al. 2018; Kojo, Jokilaakso and Hanniala 2000; Mackey 1982; Matousek 1993; Stefanova, Genevski and Stefanov 2004; Wang et al. 2013b; Yazawa 1974; Yazawa and Azakami 1969). As a result, continuously optimized flash smelting technologies have become the main copper matte production method today (Moskalyk and Alfantazi 2003).

Copper production techniques have undergone a lot of development and new equipment and processes are still emerging, such as modern continuous copper smelting and converting processes (Habashi 1995; Mackey and Campos 2001), solvent extraction-electrowinning technology (SX-EW) (Bartos 2002; Prasad, Kenyen and Assar 1992), and bottom-blown smelting and converting furnaces (Coursol et al. 2002; Liu and Xia 2019). These emerging technologies operate with good performance in production efficiency, energy-saving, and environmental protection (Bartos 2002; Coursol et al. 2002; Liu and Xia 2019; Mackey and Campos 2001). Currently, refined copper mainly comes from pyrometallurgical processes, which include matte smelting, matte converting, pyro-refining, and electrolytic refining processes. The suspension smelting and converting reactions have been analyzed (Guntoro et al. 2018; Stefanova, Genevski and Stefanov 2004; Wang et al. 2013b), but bath reactions have not yet been revealed in detail.

Bath smelting technologies can be divided into top, side, and bottom-blown technologies. Methods of setting oxygen lances at the top of the furnace are commonly used in the Top Submerged Lance (TSL) furnace (Baldock et al. 1992; Li 2009; Robilliard et al. 1994; Wood et al. 2011; Wood, Hoang and Hughes 2017) and the Mitsubishi furnace (Goto, Oshima and Hayashi 1998), but they are not the primary focus of this review. The side or bottom lances or tuyeres are all submerged beneath the surface of the melt. Side-blown furnaces typically

include Vanyukov (Vaisburd et al. 2002; Zhang et al. 2015), Teniente (Devia et al. 2019), and Noranda (Tarassoff 1984), whereas Shuikoushan (SKS) furnaces are bottom blown (Cui et al. 2010; Qu et al. 2012). Some of these bath smelting technologies are also successfully used in copper converting processes for which the Peirce–Smith (*P-S*) converter is still the most commonly used (Moskalyk and Alfantazi 2003; Southwick 2008).

The SKS technology, which emerged at the beginning of the 21st century in Asia (Cui et al. 2010; Qu et al. 2012; Shao and Jiang 2019; Wang et al. 2017a, 2017b, 2017c), has attracted growing interest. The bottom-blown copper smelting, with a current 4% share of global production (Wang et al. 2019), presents some superior characteristics to those of the FS processes. Furthermore, they have also been popularized in the copper converting process in China and may have the potential to gradually replace *P-S* converters (Liu and Xia 2019). A series of research studies on bath smelting and converting processes, especially for the SKS furnace, have been reported (Guo et al. 2016, 2015; Shao and Jiang 2019; Wang et al. 2017a, 2017b, 2017c; Wang, Guo and Tian 2017d).

The temperature of smelting or converting processes can rise to over 1200°C due to the exothermic reactions so there is no way to monitor the internal flow phenomena. Therefore, most of the visualized transport phenomena presented by scientific research are derived from simulation approaches, mainly water modeling, and Computational Fluid Dynamics (CFD) (Akashi et al. 2020; Elfsberg and Matsushita 2011; Ersson et al. 2006; Svyatoslav and Takashi 2003; Tang et al. 2017; Wang et al. 2017). X-ray radioscopic visualization is an observation method that uses a high-speed camera to capture the images of flow phenomena such as bubble motion in a liquid alloy at operating temperature (Akashi et al. 2020; Elfsberg and Matsushita 2011; Svyatoslav and Takashi 2003).

In water models, water and oil represent matte and slag because of the difference in their density and mutual immiscibility. When air is blown into the water layer, mixing behavior, bubble plumes, and surface waves appear and can be easily captured by a high-speed camera. Some experiments are combined with the PIV (Particle Image Velocimetry) technique to measure the whole 2D plane in order to describe the details of the fluid flow (Ersson et al. 2006; Wang et al. 2017). In the meantime, with the rapid development of computing power in the last 30 years, CFD software has also demonstrated a strong capacity to describe an integrated flow field in metallurgical vessels (Tang et al. 2017) allowing simulation data to be explicitly visualized, including phase distribution, velocity distribution, and mixing behavior. Currently, water modeling and CFD simulation are the two dominant research approaches for the study of transport phenomena in copper smelting and converting (Taskinen et al. 2019a, 2019b) for the optimization of industrial variables including nozzle or the tuyere number and angles, gas flow rate, and thicknesses of slag and matte layers, which have significant impacts on multiphase flow and mixing efficiency.

According to this literature review, a lot of both experimental and modeling studies on the SKS furnace, Vanyukov furnace, and *P-S* converter have been reported. Only a little research on other bath smelting or converting technologies

was reported before the mid to late 20th century when these technologies were in their development stage. Gas plumes or bubble swarms and surface waves in smelting or converting furnaces have been taken into consideration, because of their inevitable impacts on mixing efficiency and furnace lifespan. In some cases, a high gas flow rate causes strong surface waves with fierce slopping, which has been proven to accelerate lining wear (Brämning 2010; Brämning et al. 2011).

Sometimes a production technology is used in industry but no theoretical or scientific considerations have been published. For instance, the bottom-blown copper smelting furnace has been successfully used for around 10 years (Cui et al. 2010; Qu et al. 2012), but no supporting prior studies were found that predate the time of commencement. In general, the results from physical and computational modeling deserve a comprehensive review.

The purpose of this literature review is to reveal the current understanding of transport phenomena in copper bath smelting and converting furnaces. The analysis of experimental and computational modeling results would contribute to further understanding the flow phenomena that significantly affect mixing efficiency and furnace life span. The results are grouped according to the geometrical similarities instead of, *e.g.*, smelting and converting processes. Therefore, this review could be used as a reference for optimizing the production efficiency of current copper smelting and converting furnaces and contribute to the design of new reactors. Furthermore, it aims to point out possible areas for future experimental and/or modeling investigations.

2. Mixing in bath smelting and converting vessels

Generally, for furnaces with submerged tuyeres, such as bottom-blown and side-blown furnaces, the multifluid movements involved could be described as follows: in the initial blowing period, bubble swarms or gas plumes are generated when gas is injected through nozzles into the bath. These bubbles keep moving upward and drive the melt flow with them, forming a rising jet zone. As these flows move to the surface of the melt, a fountain zone will be generated with splashes and liquid droplets if the gas flow rate is high enough. The return flow from the fountain zone goes back into the melt and causes waves on the surface that keep moving to the sidewall and finally calm down after impact against the refractories. An area without any movement of gas flow or melt is called a dead zone. It is clear that reducing the dead zone area is helpful for improving the mixing efficiency of the reactants. A typical example is shown in Figure 1, which shows the flow phenomena in a water model of a *P-S* converter reported by Zhao et al. (Zhao et al. 2018). In furnaces with oxygen lances above the melt level, such as the Mitsubishi furnace, the gas impacts the surface of the melt, making a cavity beneath the oxygen lance (Nordquist et al. 2006). During this process, waves are generated and spread in a radial pattern before gradually weakening.

Using experimental and computational modeling approaches, copper smelting and converting reactors are under further optimization to improve their operational efficiency and reduce the damage to furnace structures. For example, the flow phenomena in bath copper smelting and converting vessels can be significantly changed by the nozzle and tuyere arrangement and gas flow rate.

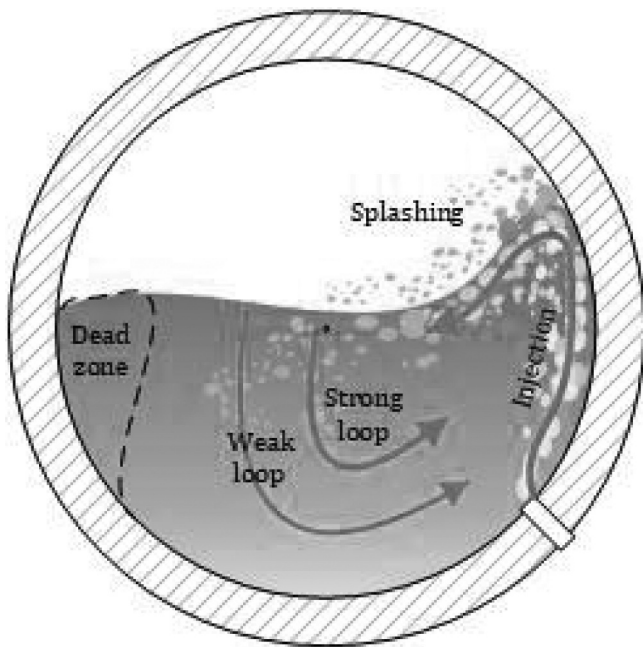


Figure 1. A schematic diagram of flow fields in a water model of a *P-S* converter, adapted from the report of (Zhao et al. 2018).

Therefore, studies concerning these parameters are reported in this section for bottom, side, and top-blown furnaces. Some results from steelmaking research that shows similarities with copper smelting and converting processes are also included.

2.1. Lance, nozzle, or tuyere arrangement

In multiple tuyere rows, the number, angle, and diameter of the tuyeres, and the distance in between them are the key parameters for bottom-blown and side-blown copper smelting and converting furnaces. Similarly, the lance height, number of nozzles, and nozzle configuration significantly affect the mixing efficiency in top-blown copper smelting and converting furnaces. Optimizing these parameters to the utmost is a very complicated task. Physical modeling and computational simulation approaches have been further developed in recent years, giving rise to a more scientific and convenient way to discover the mixing behavior of different gas blowing or injecting arrangements with nozzles, lances, or tuyeres. Therefore, it may be possible to use these approaches to improve the bath smelting and converting processes for copper production, especially for emerging technologies.

2.1.1. Experimental studies

A water model study of a bottom-blown copper smelting furnace was carried out with PIV technology to investigate its flow field characteristics (Wang et al. 2017), which reported the velocity distribution of a molten pool with nozzles installed at different angles. The nozzle angle was defined as the angle between the vertical and the nozzle axis. When the nozzle was set at 0° , dead zones appeared at each side of the bubble plume and the high-velocity area was small. When the nozzle angle was increased, the high-velocity area was expanded significantly, and the circulation area on the opposite side of the

nozzle also became stronger, making a larger dead zone in the center of the circulation. In addition, based on the results from the nozzle angles of 0° , 7° , 14° , and 22° , it was found that different nozzle angles cause very different flow patterns, but the low and high-velocity areas seem not to be affected. Another water model report from the same authors (Wang et al. 2013a) indicated that the gas holdup also changed with different nozzle angles. With an increase in the nozzle angle from 0° to 22° , there was less splashing in the bath and more bubbles appeared in the lower part of the bath.

Water modeling of a bottom-blown furnace for steelmaking processes has been reported (Chen et al. 2007; Lai, Xie and Zhong 2008) that shows some results of other nozzle arrangement parameters, such as the symmetry of the nozzle positions. Based on these experiments, an asymmetric and concentrated nozzle arrangement had a shorter mixing time than a symmetric arrangement. This conclusion might be valuable for future improvement of bottom-blown bath vessels for copper production.

The *P-S* converter has a similar operation mechanism, as it has submerged tuyeres in a horizontal cylindrical furnace. Zhao et al. (Zhao et al. 2018) used a water model with different tuyere angles and rotation directions to simulate the transport phenomena in the *P-S* converter. According to their results, the velocity distribution of the *P-S* converter is almost the same as that of the SKS furnace. However, owing to the side-blown pattern and gas injection regime which are totally different compared to the SKS furnace, experiments to optimize the operating parameters of *P-S* converter are still necessary. To describe the effect of the tuyere location, the tuyere angle was defined between the tuyere axis and the horizontal, and a positive angle corresponded to a clockwise rotation. A schematic diagram of this water model is shown in Figure 1 above. According to their observation, with an increase of tuyere angles from 0° to -15° (rotated counterclockwise), the immersion depth of the tuyeres was lower. Waves and splashing were weaker, and the mixing and mass transfer efficiency were improved. The optimized angle range was determined at less than 10° rotated clockwise based on results recorded with a high-speed camera.

A horizontal cylindrical water model study with side and bottom blow was carried out by Jiang et al. to reveal the effect of the horizontal distance between oxygen tuyeres on mixing time (Jiang et al. 2019a). In this study, the mixing time in the bottom blow model agreed well with a previous research study (Shui et al. 2015), showing the reliability of the experimental data of these two studies. According to the observations of Jiang et al., the side blow arrangement showed better mixing efficiency across the whole range of horizontal distances between tuyeres. It was confirmed that the horizontal distance between tuyeres of both the side and bottom blow arrangements should be in a certain range, outside of which the mixing time would be significantly longer.

In top-blown copper smelting furnaces such as the TSL furnace, a single lance is installed from the top of the furnace, extending below the melt surface. A water model was used to reveal the multiphase mixing behavior in this submerged top-blown reactor (Zhao et al. 2016). Different lance diameters and lance submersion depths were investigated. At a certain gas flow volume, larger lance diameters caused a longer mixing

time, because when the inlet gas flow was unchanged, the outlet gas flow was weaker. To strengthen the interaction between gas and liquid, the authors suggested that a relatively small lance diameter might be a good choice, provided that the lance life span and manufacturing cost were acceptable. In the case of various lance submersion depths, it was found that deeper submersion would enhance the gas-liquid contact and mixing efficiency. Also, as lances in top-blown furnaces have a very short lifespan (Matuszewicz, Reuter and Hughes 2010), a higher lance quality is required when a deeper position is chosen.

The Mitsubishi continuous smelting furnace is the only lance-based copper production technology using a non-submerged lance that successfully meets the requirements of the modern industry. However, no reports on its transport phenomena were found, and only some research studies from similar geometries in the steel industry have been reported. However, a water model of a vertical vessel based on a steelmaking top-blown case was reported by Nordquist et al. (Nordquist et al. 2006). As its blow arrangement is similar to the one used in the Mitsubishi furnace, the results could provide good ideas for the lance arrangement. A lance with a 1 cm diameter was used and nozzles with different exit diameters were attached to the lance according to the experimental requirements.

The effect of the nozzle diameter and lance height on the gas jet penetration depth in the melt was investigated. It was reported that the depth increased with a decreasing nozzle diameter and decreasing lance height. The effect of different nozzle diameters came from the change of gas jet impact force at the outlet of the nozzle, as the gas flow speed had to be adjusted using nozzles in different sizes. Concerning the effect of lance height, a greater penetration depth with decreasing lance height is easy to understand as it is evident that the gas flow exiting a nozzle at a high position would be weakened by the ambient atmosphere and then spread into the liquid with less penetration. Another research study that may interest Mitsubishi is a design of twisted nozzles (Yoshihiko and Yukari 2003). The twisted nozzles caused less spitting than normal nozzles when they were adjusted at a feasible angle from the results point of view. Such a design would be a reference for further control of the multiphase flow in Mitsubishi furnaces.

2.1.2. Modeling approaches

The effect of the tuyere arrangement on mixing behavior has been successfully simulated using CFD. Zhang et al. (Zhang et al. 2013) optimized the tuyere structure parameters of the SKS furnace based on CFD simulation results. A physical model was established with only one gas inlet at the furnace bottom. The Volume of Fluid (VOF) model was used to describe the flow phenomena of the multiphase flow and the Renormalization Group (RNG) k - ϵ model was chosen to simulate the turbulence characteristics. The results were generally consistent with the water model, with an average error of approximately 5%. The operational parameters should be comprehensively considered and controlled within a suitable range in order to increase the gas holdup to expand the contact area between oxygen and melt, to improve the average flow speed of the melt to accelerate the chemical reactions, and to strengthen the turbulence energy to break up large bubbles. Optimized

measures were finally determined as 0.06 m for the oxygen tuyere diameter, 17° for the tuyere angle, and 0.98 m for the horizontal distance between nozzles. The effectiveness rate of each tuyere parameter on the SKS melt pool in decreasing order is as follows: horizontal distance between nozzles, tuyere angle, and tuyere diameter.

In 2019, Shao et al. conducted the most recent CFD research on the SKS furnace, using the Euler-Euler approach to describe the gas-liquid flow and mixing behavior (Shao and Jiang 2019). For the SKS copper smelting furnace, nine tuyeres were located at the bottom and arranged in two rows. It was found that when all the tuyeres were set along the centerline, the gas holdup was higher, but the mixing efficiency was relatively low. If the two-row tuyeres were arranged at an angle exceeding 21° , the gas holdup would decrease because of the significantly shortened distance between the tuyeres and melt surface. Therefore, based on the simulation results, the tuyere angles for the two rows were recommended to be 7° and 14° . This tuyere angle optimization is slightly different from the previous work (Zhang et al. 2013), which could be attributed to the discrepancy between the physical models. According to this latest research, the chemical reaction efficiency could also be further improved by increasing the number of tuyeres. By increasing the number of tuyeres from 9 to 13, the gas holdup rose to a higher level, due to better bubble dispersion. However, the number of tuyeres could not be increased infinitely. When 18 tuyeres were used, the mixing efficiency began to decrease significantly, even though the gas holdup was kept steady. As a result, the optimal number of tuyeres was determined to be 13.

Some industrial data on the SKS furnace would help to compare modeling and practice. Currently, most of the bottom-blown copper smelting furnaces are located in China. As a technology optimized primarily by industrial experience rather than by experiments and simulation results, a series of methods have been suggested to improve production efficiency and furnace life span. The first commercially used bottom-blown smelting furnace has nine oxygen tuyeres at the bottom arranged in two rows. Five tuyeres are at a lower level at an angle of 7° and the other four tuyeres are at a higher level at an angle of 22° (Cui et al. 2010). This arrangement is not considered the optimal choice to improve mixing efficiency because the merge of melt flows would incur further wear of the side refractory. This analysis accords with a previous water model study of the bottom blown steelmaking process, which showed that the shear stress would be increased by an asymmetric tuyere arrangement (Ballal and Ghosh 1981). Perhaps a combination of tuyere angles at 7° and 14° could be a better angle arrangement, according to recently published CFD results (Shao and Jiang 2019). Another company using bottom-blown technology built a furnace with only six tuyeres (Qu et al. 2012), arranged in a straight line at the furnace bottom in order to avoid the merge of melt flows. However, the diameter of the tuyeres had to be increased to be able to blow enough oxygen into the furnace, leading to the formation of Fe_3O_4 , which congealed in an unexpected shape at the outlet of the nozzles.

CFD modeling has also been conducted to demonstrate the mixing behavior in the P - S converter. Almaraz et al. (Almaraz

et al. 2014) built two physical models, one for a single tuyere and the other for three tuyeres. Their report was intended to emphasize a detailed change in flow phenomena when the tuyere number was increased. The simulated mixing behavior in the three-tuyere bath was very similar to the results from another work on the Teniente furnace (Rosales 1999), which suggests that the flow phenomena in different side-blown furnaces are to some extent universal. According to Almaraz et al., with an increase in the number of tuyeres, the mixing behavior in a simulated bath became extremely complicated. Results showed that the flow pattern within the multi-tuyere converter changed considerably in comparison with the single-tuyere system. According to the authors, recirculation zones and localized eddies were generated in a more chaotic flow region, limiting the formation of emerging reaction sites.

A CFD study of the P-S converter focusing on macroscopic mixing efficiency was reported by Zhao et al. (Zhao et al. 2019a), including the effect of different tuyere parameters. In this study, the VOF model was used for multiphase simulation and the standard k- ϵ model was used for turbulence. It was found that a decreased tuyere diameter would enlarge the circulating area due to the increased injection velocity. This conclusion presents the common situation where a greater penetration depth and mixing efficiency will occur when smaller tuyeres are used. Additionally, setting tuyeres at the lowest level is evidently detrimental in terms of exploiting the kinetic energy of gas injection. On the other hand, a relatively low tuyere position would supply a longer trajectory for gas moving upward, thus enhancing mixing efficiency (Zhao et al. 2019a). Results from this research are strongly consistent with the experimental results from their previous water modeling experiments (Zhao et al. 2018).

A two-phase, top-blown ISASMELT furnace was modeled using CFD simulation by Zhao et al. in 2019 (Zhao et al. 2019b). Different submersion depths and lance diameters were analyzed in order to optimize the lance arrangement. The diameters were recommended to be less than 0.035 m, for the same reasons as for almost all submerged blowing situations, as the gas flow will always be weakened at the lance outlet when the diameter is increased with an unchanged gas volume. When the lance tip submersion depth was increased, the mixing time was significantly shortened because of the increased interactions between gas and liquid. Zhao et al. also investigated mixing behavior with a swirler installed in the oxygen lance near the outlet. It was found that the mixing time was dramatically shortened at a low submersion level, and maintained a similar value compared with the non-swirler when the submersion depth was increased. These results present an idea where a swirler installed in the lance might also be an option for submerged blown furnaces.

Some lance designs from the steelmaking process may be worth reviewing, such as the Top-Bottom-Side (TBS) converter with a combined top, bottom, and side blowing system (Zhou et al. 2015). From their CFD simulation results, the sidewall shear stress was found to increase due to the introduction of a side gas flow, which may cause further corrosion of the sidewall refractory. Furthermore, with the raising of the sidewall nozzle level, the interaction between the side flow and cavity flow became more intensive, resulting in a more drastic

oscillation of the bath. This research shows that a combined oxygen blow arrangement could strengthen the mixing efficiency, but problems including refractory wear and bath oscillation may also occur because of the effect of the side gas blow.

He et al. conducted CFD modeling of a steelmaking top-blown converter, using the VOF model and the standard k- ϵ model to describe the mixing behavior in the multiphase system (He et al. 2011). The model has a non-submerged lance installed with four outwardly inclined nozzles at a small angle. As a top-blown case with a non-submerged lance, this could contribute to the design of a Mitsubishi lance structure and arrangement. As in a top-blown water model (Nordquist et al. 2006), a lower lance height is beneficial for lowering the penetration depth. It was also found that a lance at a lower position was able to have a positive influence on the velocity of melt flows in the top section of the bath, whereas gas from a lance at a higher position would optimize the homogeneous distribution of the velocity in the radial direction. Similar discrepancies also appeared in similar research by Cao et al. (Cao et al. 2018). Such options regarding lance height may be common for both the top-blown copper smelting or converting process and the top-blown steelmaking process.

2.2. Gas flow rate

In industrial practice, the gas flow rate or gas injection pressure is an important parameter for the adjustment of production efficiency. High mixing efficiency in the bath always requires a relatively high gas flow rate. However, it cannot be increased infinitely, and should be kept within an appropriate range, because a very high gas flow rate causes intense splashing of the melt surface, thus damaging the sidewall refractories. On the other hand, a very low gas flow rate is not able to supply adequate kinetic energy to mix the reactants. Sometimes even a low gas flow rate can lead to lining wear in a bottom-blown furnace, because some of the gas bubbles at low velocity tend to accumulate in the nozzle area, resulting in an acceleration of corrosion reactions on the refractory surface (Yu et al. 2013). In this section, the effect of different gas flow rates on copper smelting and converting processes is described, which can help in finding ways to further optimize mixing behavior.

2.2.1. Experimental studies

In general, a higher gas flow rate brings stronger kinetic energy to the smelting or converting system, which accelerates the multiphase flow and improves the mixing efficiency. Using potassium chloride as a tracer in a water model of bottom-blown copper smelting, Shui et al. proved that increasing the gas flow rate did indeed make a significant improvement in both the mixing efficiency and effective stirring range (Shui et al. 2015). A detailed description derives from the PIV measurements of the water model of a bottom-blown furnace carried out by Wang et al. (Wang et al. 2017). They found that increasing the gas flow rate could improve the mixing of a multiphase flow, enhance the circulation, and reduce the dead zone. When the gas flow rate increased to a certain value, the most homogeneous flow field would appear in the melt pool, where only a small narrow dead zone existed near the backflow zone next to each side of the furnace wall. They believe that the appearance of a small dead

zone and low-velocity area is inevitable, even at a relatively high gas flow rate, owing to the existence of a circulation zone and backflow collision. Moreover, the gas flow rate should not be increased infinitely, as it would also cause fierce splashing which always leads to the corrosion of sidewall refractories and a sharp decrease in the furnace life span.

In the *P-S* converter, oxygen is injected into the melt in a bubbling regime rather than a jetting regime, which means that the gas inside moves upward in a nearly vertical direction without further immersion and the gas velocity is regulated within a relatively low range. However, as reported by Zhao et al., an increasing gas flow rate increases the immersion depth and the volumes in the injection regions and in the strong loop, and also homogenizes the distribution of the gas-liquid phase and bubbles (Zhao et al. 2018). Undoubtedly, with an increased gas flow rate, spitting and splashing would be intensified, causing more damage to the sidewall. Additionally, another negative outcome was also confirmed: the gas outflow simultaneously increased, which indicated a decline in the gas utilization rate.

The mathematical characterization and water model verification of the gas jet penetration depth of the side blow pattern were reviewed and further studied by Kapusta (Kapusta 2017), focusing on a comparison between bubbling and jetting regimes. The occurrence of both gas flow regimes depends on the adjustment of the oxygen flow rate. The results showed that the high-speed gas flow in the jetting regime caused a longer penetration depth and gas trajectory than the conventional blow arrangement, such as in the Noranda and Teniente reactors, which might be a feasible method for improving the mixing efficiency (Kapusta 2017). According to Kapusta, a real case that has been proven successful is the practice of the converting process at Glencore Nickel in Canada. This research shows the possibility that a smelting or converting furnace in a bubbling regime with conventional low gas injection and side tuyeres could be modified to a furnace with a jetting regime, without the necessity to build a new furnace to replace the old one.

Results from water model experiments on the Argon–Oxygen Decarburization (AOD) converter in steelmaking could be examined so as to understand the mixing phenomena in the side-blown copper smelting/converting furnace. Bjurström et al. investigated the effect of the gas flow rate and bath height on the plume penetration depth (Bjurström et al. 2006), which was defined as the horizontal distance from the gas inlet side at the level of the tuyere and the vertical distance from the level of the bath surface, respectively. A general point from their observations was that the gas flow rate was the key factor that predominantly influenced the penetration depths of the gas plume in both the tuyere area and the surface area. At a relatively high gas flow rate, the penetration depth became lower and the recirculation loop generated in the corner of the bath tended to move closer to the sidewall opposite the injection point. Ma et al. (Ma et al. 2016) empirically predicted the relation between the penetration depth (H_p) and relevant operating parameters of the side blow as:

$$H_p/D = 0.13Fr^{0.075} \left(\sqrt{\frac{\rho_g}{\rho_l}} Re \right)^{0.43}, \quad (1 < Fr' < 30). \quad (1)$$

This formula agreed well with experimental data from various research studies (Iguchi et al. 1993; Kulkarni and Joshi 2005;

Ma et al. 2016). Based on equation (1), the Fr' and $\rho_g^{0.5} \rho_l^{-0.5} Re$ are two important dimensionless numbers influencing the penetration depth, both of which are related to the gas flow rate.

According to the results from Zhao et al., the effect of the gas flow rate is basically the same for a submerged blow from the top or from the side (Zhao et al. 2016). A higher oxygen rate would also intensify the splashing and waves on the melt surface. For TSL furnaces, both oxygen flow rate and lance depth should be regulated in an appropriate range to avoid unexpected refractory wear. The mixing time T_{mix} could be expressed as Equation (2):

$$\begin{cases} T_{mix} = 0.06H^{0.85}D^{0.75}h^{-0.65}Q^{-2}Q \leq 0.0125\text{m}^3 \cdot \text{s}^{-1} \\ T_{mix} = 2140H^{0.85}D^{0.75}h^{-0.65}Q^{0.4}Q > 0.0125\text{m}^3 \cdot \text{s}^{-1} \end{cases} \quad (2)$$

Ersson et al. (Ersson et al. 2006) conducted experiments using PIV technology to determine the effect of the gas flow rate on the recirculation loop in the water model of a combined top and bottom-blown vertical reactor. It was confirmed that the top blow was able to create a small recirculation loop beneath the water surface. With an increase in the gas flow rate, this loop moved downward regardless of whether there was a top or bottom blow arrangement. When the gas flow rate was further increased, the recirculation area became difficult to distinguish.

2.2.2. Modeling approaches

The effect of the gas flow rate on the mixing phenomena in a bottom-blown copper smelting furnace was reported by Shao et al., using CFD modeling results (Shao and Jiang 2019). The physical modeling was arranged with 13 tuyeres on the bottom with nine and four tuyeres in rows A and B, respectively. The angles between the vertical and the tuyeres were 1° for row A and 7° for row B. The visualized simulation results showed that, with an increase in gas flow rate, the gas volume fraction in two bubble plume zones gradually increased and the height of the standing wave also rose. When the gas flow rate exceeded $18.8 \text{ m}^3 \cdot \text{h}^{-1}$, the two bubble plumes tended to overlap and combined into a single large stream. The total gas volume in the bath would increase at a relatively slower speed because of the tendency of bubble plumes to overlap.

As already discussed in this review, an increasing gas flow rate may cause an intense flow and splashing in the *P-S* converter. However, it seems that the mixing efficiency shows a different trend. Chibwe et al. systematically conducted a series of three-phase CFD simulations on the *P-S* converter using the VOF model and the realizable *k-ε* model (Chibwe 2011; Chibwe et al. 2013). It was found that the mixing efficiency coefficient increased with an increasing gas flow rate in a certain range, then tended to decline even at a higher gas flow rate (Chibwe 2011). According to the CFD results (Chibwe 2011), this phenomenon could be attributed to a channeling process, during which injected gas went straight to the surface of the melt without the possibility of recirculation and mixing. In addition to the decreased mixing efficiency due to channeling, the dispersion between slag and matte was also found to be affected by different gas flow rates (Barron et al. 2010; Chibwe et al. 2013). Based on the simulation results, with an increased gas flow rate the dispersion of matte in slag would increase,

whereas the dispersion of slag in matte would decrease. The mechanism of this phenomenon requires further investigation.

Mostly, the method of gas injection operating in *P-S* converters is the bubbling regime, which can also be transformed into the jetting regime at a relatively high gas flow rate, if necessary. In practice, a plant trial has been carried out to examine the feasibility of the jetting regime in the *P-S* converter (Brimacombe, Meredith and Lee 1984). It was proved that the tuyeres were able to accommodate a high-pressure gas blow, indicating that the *P-S* converter does have the potential to operate with the jetting regime, which may significantly improve the mixing efficiency. To estimate the boundary between the bubbling and jetting regimes, Barron et al. conducted a series of specific CFD modeling studies on the transition between the regimes at different gas flow rates in the *P-S* converter (Barron and Hernandez 2016; Barron et al. 2010). A simulated multiphase flow was investigated at gas flow rates of $5 \text{ m}\cdot\text{s}^{-1}$, $50 \text{ m}\cdot\text{s}^{-1}$, and $100 \text{ m}\cdot\text{s}^{-1}$. An injection air jet flow rate of $5 \text{ m}\cdot\text{s}^{-1}$ led to the bubbling regime and slight stirring in the bath. When the airflow rate was increased to $50 \text{ m}\cdot\text{s}^{-1}$, the bubbling regime persisted even though significant stirring and intense splashing occurred. These phenomena seemed to take place as a transition between the bubbling and jetting regimes. At an airflow rate of $100 \text{ m}\cdot\text{s}^{-1}$, the jetting regime replaced the bubbling regime and the splashing became fierce. To quantify this transition, the Kutateladze number, which is defined as

$$\text{Ku} = \frac{U \sqrt{\rho_g}}{(\sigma g (\rho_l - \rho_g))^{0.25}}, \quad (3)$$

was introduced as a quantified reference to estimate the airflow regime in the *P-S* reactor (Barron et al. 2010; Sundar and Tan 1999). The Ku was then calculated based on numerical simulation results at an injection velocity of $5 \text{ m}\cdot\text{s}^{-1}$, $50 \text{ m}\cdot\text{s}^{-1}$, and $100 \text{ m}\cdot\text{s}^{-1}$, showing that the transition of the bubbling regime to the jetting regime would take place when the Ku exceeded 3.4832 (corresponding to a gas flow rate of $50 \text{ m}\cdot\text{s}^{-1}$).

The effect of gas flow rate on a side-blown copper smelting furnace has also been investigated. Zhang et al. reported CFD simulation results of a multiphase flow in the Vanyukov furnace (Zhang et al. 2015). The VOF and the standard *k-ε* models were used to describe the multiphase flow and turbulence, respectively. The phase distribution, velocity distribution, and the relation between the gas flow rate and the slag velocity were determined. With the increase in gas flow rate from $70 \text{ m}\cdot\text{s}^{-1}$ to $160 \text{ m}\cdot\text{s}^{-1}$, the velocity of the slag above the tuyeres improved significantly. Furthermore, it was found that along the line from the tuyeres to the furnace centerline, the slag velocity first improved to a peak value and then decreased. This peak velocity area tended to move toward the furnace centerline when the gas flow rate became higher. As the higher gas flow rate was able to intensify the slag movement and slag/exhaust duct interface waves, the authors deduced that it is possible to enhance desulfurization by increasing the gas flow rates. Due to the demand for refractory protection, the gas flow rate should be within a controlled range. To further increase mixing efficiency, Valencia et al. conducted CFD modeling on a Teniente converter, indicating that extra

tuyeres could be installed at the bottom, which would increase the integral gas flow rate and would not break the stability of the whole bath (Valencia, Rosales-Vera and Orellana 2013).

In the ISASMELT furnace, according to the CFD modeling work of Zhao et al., the mixing time generally decreases with an increasing gas flow rate (Zhao et al. 2019b). A noteworthy point is that, in this case, as the gas flow rate increased to a certain range, mixing would become relatively slow. This could be attributed to the intensified splashing which, in turn, limits the applicability of a high gas flow rate. Hence, there is an optimal range of gas flow rate as regards the mixing time. In general, if the slowing of the mixing process is indeed a result of the fierce splashing, it is reasonable to assume that a similar situation may also exist inside or bottom-blown copper smelting and converting furnaces. To test this assumption, further modeling work is required. However, researchers are currently mainly concentrating on eliminating splashing to reduce refractory wear when the gas flow rate is increased.

2.3 Slag and matte layer characteristics

Mixing efficiency is affected by bath height, slag layer thickness, and slag characteristics such as kinematic viscosity. Currently, the effect of slag and matte layer characteristics is mostly being considered in the water model research on bottom-blown furnaces and CFD studies of the *P-S* converter. The experimental and simulated results of these research studies are discussed in this section.

2.3.1 Experimental studies

The effect of the bath height on the mixing efficiency of an SKS furnace has been investigated by Wang et al. by conducting PIV measurements on a horizontal bottom-blown water model (Wang et al. 2017). It was confirmed that an increased bath height would contribute to decreasing the dead zone, increasing the mean velocity, and contributing to the reduction of splashing and instability. Therefore, basically the effect of increasing the bath height would be positive in terms of mixing efficiency. According to another water model study from Shui et al. (Shui et al. 2015), the increase in bath height also helped to reduce the mixing time and increase the mixing efficiency within the effective stirring range. At a certain bath height, only a slight variation in mixing time was detected between the surface, middle, and bottom of the bath. However, when the bath height increased, the mixing time decreased rapidly within a limited range, and then tended to decrease at a slower rate if the bath height kept rising. Based on the analysis of the experimental results, they suggested that, in certain conditions, the mixing time T_{mix} in a bottom-blown water bath could be expressed as a function of gas flow rate Q and bath height H :

$$T_{mix} = 0.0608Q^{-0.39}H^{-1.08} \quad (4)$$

A similar relation between T_{mix} , gas velocity and bath height was also reported in steelmaking ladle modeling studies, and the results are shown in Table 1.

In Table 1, the exponent number of Q or \mathcal{E} for horizontal bottom-blown vessels is -0.39 and H is -1.08 , while for vertical bottom-blown vessels the exponent number of Q or \mathcal{E} is in the

Table 1. A comparison of T_{mix} expressions in horizontal and vertical bottom-blown vessels with a single nozzle.

Horizontal vessel	$T_{mix} = CQ^{-0.39} H^{-1.08}$	(Shui et al. 2015)
Vertical vessel	$T_{mix} = C\mathcal{E}^{-0.33} D^{1.36} H^{-1}$	(Asai et al. 1983)
Vertical vessel	$T_{mix} = C\mathcal{E}^{-0.33} D^{1.66} H^{-1}$	(Mazumdar and Guthrie 1986)
Vertical vessel	$T_{mix} = CQ^{-0.47} D^{1.97} H^{-1} v^{0.47}$	(Iguchi, Nakamura and Tsujino 1998)
Vertical vessel	$T_{mix} = CQ^{-0.217} D^{1.49} H^{-1} v^{0.37} [(\rho_l - \rho_g)/\rho_l]^{-0.243}$	(Yamashita et al. 2003)

^aTo make a visual comparison, the formulas of T_{mix} in Table 1 have been simplified. C is a constant number that can be changed in different conditions and units, \mathcal{E} is the mixing power density that is proportional to the gas flow rate Q , v is the kinematic viscosity of liquid, and ρ_l and ρ_g are the density of liquid and gas, respectively.

range of -0.47 to -0.217 and H is -1 for all. This indicates that the effect of the gas flow rate on mixing time in horizontal bottom-blown vessels, such as SKS furnaces, is on a corresponding level with that of vertical bottom-blown vessels, whereas the effect of bath height is more significant in horizontal than in vertical vessels.

Transport phenomena are also strongly associated with the characteristics of the slag layer. To simulate the effect of slag in a bottom-blown vessel, Shui et al. conducted water model experiments using oil to simulate the slag (Shui et al. 2018a). The effect of the oil layer thickness and viscosity on the mixing time was investigated. When the thickness of oil was less than the critical value, a change in oil thickness seemed to be unrelated to the mixing time. However, when the oil thickness increased over this range, the mixing time increased significantly. An increase in the gas flow rate might be feasible to shorten the mixing time in the case of a thicker slag layer. It was found that the thickness of the slag would change the sensitivity of mixing time toward different gas flow rates. The decreasing rate of mixing time in a thicker oil system was significantly larger than that in a thinner oil or oil-free system. This indicated that an increase in the gas flow rate may be more effective when the slag phase becomes thicker, and contradictory to intuition and other results, the thicker slag layer appeared to promote mixing efficiency when the gas flow was increased.

Slag viscosity is also an important property as it always affects the smelting or converting process chemically or physically. According to one research study (Shui et al. 2018a), the higher kinematic viscosity of oil causes a longer mixing time. However, in comparison with the impact of a change in oil thickness, the oil viscosity corresponding to slag viscosity had relatively less influence on mixing time. This to some extent coincides with the T_{mix} expression from Iguchi et al. given in Table 1, as the absolute value of the exponent constant for kinematic viscosity is around half as much as that for bath height.

Bath height is considered as a variable in the top-blown water model research of Zhao et al. (Zhao et al. 2016); mixing time expressed as a function of bath height as shown in section 2.2.1. From their observations, an increase in bath height would prolong the mixing time in top-blown vessels, which is different from what occurs in bottom-blown vessels. It is evident that the whole volume of liquid will be increased when the bath height rises, and tracers such as KCl, commonly used for measuring the mixing time, will need more time to spread.

2.3.2 Modeling approaches

Chibwe (Chibwe 2011) conducted a CFD simulation of the P-S converter using the VOF model and the realizable k- \mathcal{E} model to describe multiphase turbulence behavior. In the model, the mixing time increased with increasing simulated slag thickness, and the expression of mixing time T_{mix} was

$$T_{mix} = 30722Q^{1.35}S^{-0.08}. \quad (5)$$

Another CFD research study (VOF and realizable k- \mathcal{E}) from Chibwe et al. (Chibwe et al. 2015) gives a detailed description of the effect of slag thickness on the mixing phenomena in the P-S converter. The simulation results are in good agreement with their water model experiment (Chibwe et al. 2015); in the water modeling with different slag thicknesses, the mixing time showed the reverse tendency. Specifically, if the slag was thicker than a certain value, which could be a critical point, an increasing gas flow rate would extend the mixing time, whereas if the slag thickness was lower, i.e., below that critical value, the mixing time would show a decreasing trend with an increasing gas flow rate. The authors explained this discrepancy visually using numerical simulation results. With a relatively thinner layer, the slag was almost all pushed to the opposite side of the tuyere line, with only the matte phase remaining in the gas plume zone. The density of matte is higher than that of slag, which means that the pressure on the rising bubbles is increased and the bubble retention time is prolonged. Therefore, when the slag thickness is in this thinner range, a higher gas flow rate contributes to improving the mixing efficiency. When the slag layer was thickened beyond this range, the effect of interaction and dispersion was stronger and localized recirculation became more significant. This led to energy dissipation and resulted in the extended mixing time.

3. Gas plumes, bubble swarms, and surface waves in bath smelting and converting

3.1. Phenomena of gas plumes and bubble swarms

Kulkarni et al. reported a comprehensive review of bubble formation and bubble rise velocity in gas-liquid systems (Kulkarni and Joshi 2005) with a detailed description of their observation methodology, associated variables, mechanisms, and mathematical expressions. However, the bubble behavior in different vessels may be different. In this section, the modeling results of gas plumes and bubble swarm characteristics in copper smelting and converting furnaces or similar reactors are presented. Currently, research on bubble behavior in copper smelting and converting processes conducted with physical model experiments and computational simulation mostly focus on bottom-blown vessels.

3.1.1. Experimental studies

Oxygen-enriched air is blown into SKS furnaces in the jetting regime, but not in the bubbling regime, which is adopted in most side-blown copper smelting or converting furnaces. For the jetting regime, air blown into the bath is separated into small bubbles with a large specific surface area, which further increases the interaction between gas and liquid. Furthermore, small bubbles also help to weaken the spitting which could

cause damage to the sidewall lining. Therefore, to increase mixing efficiency and reduce refractory erosion, the bubble diameters need to be controlled within a small range. Wang et al. conducted water model research on the bubble diameter in a bottom-blown vessel, using a high-speed camera to record bubble images continuously (Wang et al. 2016). Based on the experimental data, the relation between the bubble diameter d_B , nozzle diameter D , angle between nozzle and horizontal plane θ , and gas velocity U was empirically developed and expressed as follows:

$$d_B = 0.41666D^{0.29374}\theta^{-0.46572}U^{-0.16725}. \quad (6)$$

In this equation, the absolute value of the exponent number of θ is the largest, which means that the nozzle angle is the most powerful factor affecting the bubble diameter. To decrease the bubble diameter, a smaller nozzle diameter, larger nozzle angle, and higher gas flow rate are proposed. However, apart from the conclusions from the experiments, the authors also expressed concern about the reliability of their water model results when compared with real smelting processes for the following reasons: first, the oil and water density and surface tension are different from those of slag and matte, and, second, bubbles moving upward might undergo a temperature increase, which would probably cause significant discrepancies in the bubble motion between water models and industrial furnaces.

The plume eye in a bath is another phenomenon that raises concern. With a relatively thin slag layer, lower density slag is usually pushed away by the gas plumes and bubble swarms moving upward, and the higher density matte is exposed. The area of matte or deeper layer exposure is referred to as the plume eye. The size of the plume eye should be optimized, because, on the one hand, a large plume eye can reduce the copper remaining in the slag, but, on the other hand, it also leads to the acceleration of lining corrosion. A water model experiment on the plume eye in a single nozzle water model of an SKS furnace was carried out by Jiang et al., who presented the changes in the plume eye size in different conditions (Jiang et al. 2019b). They confirmed that the area of the plume eye expanded with an increasing gas flow rate and thinning of the lower layer, whereas it shrank with a thickening upper layer. To predict the characteristics of a plume eye specifically, a model was created and is described as:

$$\frac{A_{es}}{H_l^2} = 0.45 \left(1 + \frac{H_u}{H_l}\right)^2 \left[1 - \frac{2H_u g}{U_p^2}\right]^2 \quad (7)$$

$$U_p = 16Q^{0.33}H_l^{0.25}R_e^{-0.58} \quad (8)$$

$$R_e = \sqrt{\frac{R^2 \arccos\left(\frac{R-(H_u+H_l)}{R}\right) - \sqrt{2R(H_u+H_l) - (H_u+H_l)^2}(R - (H_u+H_l))}{\pi}} \quad (9)$$

from which the predicted value generally agreed with the experimental results and can probably be used to predict the size of the plume eye in bottom-blown furnaces.

Akashi et al. (Akashi et al. 2020) observed the bubble behavior in a TSL top-blown furnace using an X-Ray radioscopic visualization method. Compared with water modeling processes, this observation approach can provide information on bubbles that is closer to the real situation, because of the liquid alloy used as a substitute for water. It was found that with an increasing gas flow rate, the mean equivalent bubble diameter increased, and when the gas holdup increased, the interactions between bubbles became more frequent, creating a growing number of small bubbles as a result of the bubble breakup and gas entrainment. A higher gas flow rate and lower lance submersion depth produced the largest number of bubbles of various sizes, which would significantly promote the reaction efficiency. These results show great similarity with a top-blown water model (Zhao et al. 2016) and, furthermore, present a more specific illustration of bubble behavior.

3.1.2. Modeling approaches

Zhang et al. (Zhang et al. 2016) conducted a CFD simulation of a simplified bottom-blown physical model of an SKS furnace in a Chinese company. The simulation results (VOF and RNG k- ϵ) showed improved performance of a complicated multiphase flow, such as swirls appearing in the SKS furnace bath, and they were well in line with the water model verification experiments. According to the water model photographs and visualized CFD results, bubbles underwent two stages before their ultimate formation. In the first stage, a bubble with an increasing diameter appeared, attached to a tuyere outlet. During the second stage, the bubble grew further, and consequently buoyancy increased, and the bubble started to move upward. The connection between the bubble and the tuyere outlet was not cut, due to the necking formation between them. As air or oxygen-enriched air was blown continuously, the bubble size became larger and the necking was also prolonged until the bubble detached from the tuyere. In the lower section of the bath, bubbles moved at a relatively low speed with less possibility for interacting with each other. In the upper section, as the pressure from the upper layer lessened, the rising velocity of the bubbles increased. This contributed to the aggregation and breaking of the bubbles in the bath. The broken bubbles dispersed into the surrounding liquid and stayed for a longer time, increasing the gas holdup from 10% to 39% in the SKS water model. Therefore, based on the behavior of bubbles in the lower and upper sections of the bath, the region of higher reaction efficiency is highly likely to be in the upper bath area.

In the case of gas injection in the bubbling regime, the research on P - S converter modeling is an example of describing the motion of bubbles (Vaarno et al. 1998). The tuyere angle of the P - S converter is between that of the side-blown and bottom-blown furnaces. However, because of the bubbling regime, the P - S converter shows more similarity with side-blown furnaces such as Teniente and Vanyukov reactors, in terms of bubbles. According to the photographs from the water model experiments, air injected from a tuyere move upward, adjacent to the sidewall after leaving the outlet, generating individual bubbles that then break up into bubble swarms. The results of computational simulation showed a similar

phase and velocity distribution to the water model, although it also revealed some differences.

In the *P-S* converter, the simulated distribution of the bubble swarm void fraction is sharper than that of the water model. The calculation results indicated that the gas fraction in the core of the bubble swarm is too high to be a simple bubble dispersion, and is more of a frothing or foaming process. A low proportion of matte in the core of the bubble swarm may cause a high local matte oxidation rate, and re-reduction of the oxidized matte in the recirculation zone. Therefore, the authors (Vaarno et al. 1998) believe that the bubble formation stage is probably the best time for oxidation, and the majority of matte oxidation takes place near the tuyeres where the oxygen initially meets the matte. The optimal reaction zone in the *P-S* converter or other side-blown reactors operating in the bubbling regime seems completely opposite to that of SKS furnaces.

3.2. Surface waves

Making the bath surface behavior controllable will contribute to reducing slopping with less impairment of mixing efficiency. The occurrences of transversal and longitudinal standing waves have been investigated for the optimization of copper smelting and converting reactors (Liow and Gray 1990; Rosales et al. 2003; Shui et al. 2016, 2018b). So far, almost all research data on the behavior of waves come from water model experiments. To make the experimental conditions closer to industrial practice in the copper making, it is worth exploring computational simulation.

Kootz and Gille (Shui et al. 2016) categorized different transversal standing waves as the first asymmetric standing wave, the first symmetric standing wave, and the second asymmetric standing wave, based on their observation of the model of a *P-S* converter. Schematic diagrams for the 1st asymmetric, 1st symmetric, and 2nd asymmetric standing wave are shown in Figure 2.

3.2.1. Experimental studies

According to the study of Shui et al. (Shui et al. 2016), three types of waves were found in a bottom-blown water model vessel without the 2nd asymmetric wave, i.e., ripples only, the 1st asymmetric wave, and the 1st symmetric standing wave. These waves developed at different gas flow rates and nozzle angles. The ripples appeared with a low gas flow rate, as the gas

plume rose almost vertically with comparatively little impact on the bath surface. At a lance angle of 7°, 15°, or 20°, since the gas flow rate exceeded the critical value the gas plume started to rotate, forcing the bath to swing following its rotation, thereby inducing the 1st asymmetric standing wave. When the lance angle was increased to 25° and the gas flow rate was adjusted to a high value, the rotation made the bath swing in a different manner. With the contribution of the gas plume, the 1st symmetric standing wave appeared.

In general, the 1st asymmetric standing wave has a much higher amplitude than both the 1st standing symmetric wave and ripples. The amplitude, therefore, increased with a decreasing lance angle, as the 1st asymmetric standing wave tended to appear at a lower angle range (Shui et al. 2016). Nevertheless, it was also found that the amplitude increased with a higher bath height and gas flow rate. Since a higher amplitude is reflected in a strengthened flow motion in the bath, these results would be in accordance with the research on the factors that influence mixing time, described in section 2.3.1. The frequency of the 1st asymmetric standing wave was found to be related to the bath height alone, namely, it slightly increased with the bath height. Experimental results of the 1st asymmetric standing wave frequency in the bottom-blown vessel from Shui et al. agreed well with a standing wave frequency evaluation (Rosales et al. 2003) expressed as

$$\alpha = \sqrt{\frac{n\pi}{4(\eta(1-\eta))^{\frac{1}{2}}}} \tanh \sqrt{\frac{n\pi}{2} \left(\frac{\eta}{1-\eta}\right)^{\frac{1}{2}}} \quad (10)$$

which was established from research on the Teniente converter.

To reveal the conditions for the existence of the 1st asymmetric standing wave, two sub-boundaries were proposed (Shui et al. 2016) that can be expressed as follows:

Sub-boundary 1: $H/R = 0.036Fr'^{-0.1}\alpha^{0.084}$, modified Froude number:

$$Fr' = \frac{Q_{mL}^2}{gR^5}, \quad (11)$$

Sub-boundary 2: $H/R = 0.63We^{0.44}\alpha^{-0.39}$, Weber number:

$$We = \frac{\rho_l Q_{mL}^2}{\sigma R^3} \quad (12)$$

Unlike transversal standing waves, a longitudinal wave continuously impacts the side refractory and is strongly associated with slag tapping and the matte droplets entrapped in the slag

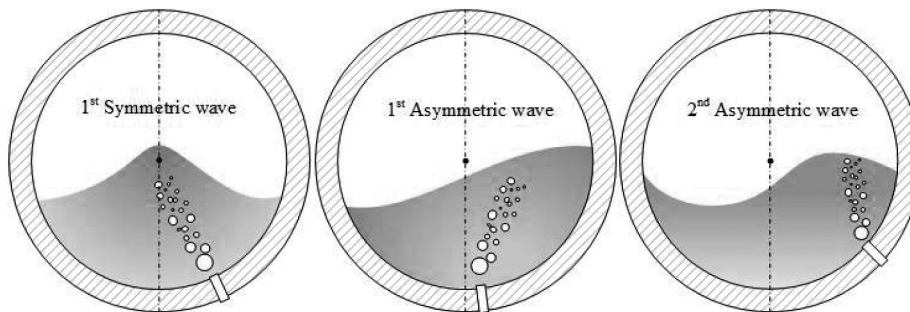


Figure 2. Schematic diagram for the 1st asymmetric standing wave, 1st symmetric standing wave, and 2nd asymmetric wave, which may occur in water models of the *P-S* converter and the SKS furnace, adapted from the report of Kootz and Gille in 1948, referred to in (Shui et al. 2016).

layer. The amplitude and frequency of longitudinal waves in the bottom-blown water model were also investigated by Shui et al. (Shui et al. 2018b). The phenomena at the bath surface with different water and oil levels were observed and recorded. When the gas flow rate was in the range corresponding to that commonly used in industrial practice, the amplitude of the longitudinal wave increased with a higher water level and remained comparably steady with a change in oil level. It was also observed that the amplitude was higher at the tapping end compared with the center. The frequency was not affected by the water level, oil level, or oil viscosity. When the bath height and gas flow rate were improved to the critical condition, the 1st asymmetric standing wave occurred, for which the frequency can be predicted using Equation (10).

Liow and Gray conducted water model experiments to investigate the formation of standing waves in the *P-S* converter (Liow and Gray 1990). The 1st asymmetric and the 1st symmetric standing wave, the 2nd asymmetric standing wave, and the longitudinal standing wave were found to be present during the gas-blowing process. It was confirmed that the occurrence of these waves was determined by the bath height and gas flow rate. Furthermore, in certain conditions, when these two parameters were adjusted to a certain range, splashing was weakened and the standing waves tended to disappear, suggesting that the gas flow rate in the *P-S* converter could be optimized within this special range to improve mixing efficiency, simultaneously limiting the effect of splashing on the side wall lining.

A theoretical prediction of the period of the standing wave was carried out using the linear wave theory (Liow and Gray 1990). The predicted value basically agreed with experimental observations in a wide range of bath heights. After an analysis of wave frequency, it is recommended that a steeper sidewall be used to increase the standing wave frequency, from which the resonance caused by gas injection would be reduced and sloping could be weakened.

4. Summary and conclusions

The published reports concerning transport phenomena in copper bath smelting and converting furnaces were reviewed in this work. The effect of the nozzle arrangement, gas flow rate, bath layer characteristics, and details including bubble motion and surface waves were systematically discussed. A summary of the research papers cited in this review is shown in Table 2.

The effect of nozzle and tuyere arrangements on mixing efficiency has been widely investigated. For the SKS furnace, in general, an asymmetric and concentrated arrangement has been confirmed to be positive for reducing the mixing time. The current number of tuyeres and their inclination angle are limiting and the mixing time and gas holdup cannot be optimized. Therefore, a combination of tuyere inclination angles of 7 and 14 degrees with a total of 13 tuyeres (which is more than previously used) is recommended. For the *P-S* converter, as a relatively small tuyere angle would supply a longer trajectory for bubbles, the optimized angle range that would weaken splashing and improve mixing efficiency is suggested to be less than 10°, rotated clockwise. For top-

blown furnaces, a smaller lance or nozzle diameter and deeper lance tip position strengthen the mixing process, but the life span of the lance has to be taken into consideration.

Increasing the gas flow rate generally contributes to the mixing efficiency in bath smelting and converting systems. Research on the *P-S* converter indicated that it is possible to transform a bubbling regime into a jetting regime by increasing the gas flow rate to achieve a greater penetration depth and longer jet gas trajectory. However, an infinitely high gas flow rate is not reasonable. According to water model research on SKS furnaces, a relatively high gas flow rate was found to be unable to eliminate the dead zone, which suggests that a higher flow rate is not always effective and sometimes results in low efficiency. Reports from studies of side- and top-blown furnaces also indicated that the gas flow rate should be kept within a certain range. A novel method to further increase the gas flow rate was proposed in a CFD study of the Teniente converter, showing that extra tuyeres installed at the bottom of the furnace would increase the integral gas flow rate and without compromising the stability of the bath.

The characteristics of the slag and matte layer were found to be related to mixing efficiency. A greater bath height improved the mixing efficiency of bottom-blown furnaces, but impaired that of top-blown furnaces. As for the effect of slag thickness, research on the *P-S* converter indicated that the mixing time would not continue increasing or decreasing with a change in slag thickness, but that a critical value existed. On either side of this critical point, the mixing time showed different trends with an increasing gas flow rate.

To increase the mixing efficiency and reduce the corrosion of the sideling, the bubble diameter should be small. Based on the observations of the bubble behavior in the SKS furnace and the *P-S* converter, the region of higher reaction efficiency is probably located in the upper bath area for reactors in the jetting regime. In contrast, for reactors in the bubbling regime, the formation of bubbles occurring at the tuyere outlet was considered as the best stage for oxidation.

In the research on both bottom blown and side blown vessels, the frequency of the 1st asymmetric standing wave, which is of higher amplitude, was found to be solely related to the bath height. In the *P-S* converter, when the bath height and gas flow rate were in a certain range, the standing wave tended to disappear with weaker splashing. This indicated that a special condition range may exist in bath smelting and converting reactors in which the mixing efficiency has the potential to increase with further adjustments to the gas flow rate and bath height.

As a conclusion, the following factors and parameters seem to warrant further research:

- In the reported CFD modeling work on the SKS furnace, the effect of slag characteristics on mixing phenomena was ignored. Therefore, an investigation of high-temperature slag characteristics for SKS technology should be conducted first.
- Simulation work on the transport phenomena of Noranda and Mitsubishi technology is not of sufficient

Table 2. Reports on the transport phenomena in copper making furnaces cited in this review.

Authors (Ref.)	Modeling Geometry/Reactor	Approaches	Research objects	Main finding
Wang et al. 2017	A slice model of SKS furnace with single nozzle	Water model with PIV technology	Mixing behavior	The effect of nozzle angle, gas flow rate, and bath height on velocity distribution
Wang et al. 2013a	A slice model of SKS furnace with single nozzle	Water model	Average diameter of bubbles	An empirical formula of average bubble diameter
Shui et al. 2015	A single nozzle model of SKS furnace	Water model	Mixing behavior	The effect of gas flow rate and bath height on mixing time
Shui et al. 2018a	A single nozzle model of SKS furnace	Water model	Mixing behavior	The effect of operational parameters on mixing efficiency with the existence of a slag layer
Shui et al. 2016	SKS furnace	Water model	Surface wave	The formation and characteristics of standing waves
Shui et al. 2018b	SKS furnace	Water model	Surface wave	Amplitude and frequency of surface longitudinal waves
Zhang et al. 2013	SKS furnace	CFD	Tuyere structure parameters	An optimized tuyere arrangement
Zhang et al. 2016	SKS furnace	CFD	Bubble behavior	The relation between mixing efficiency and bubble characteristics
Shao and Jiang 2019	SKS furnace	CFD	Mixing behavior	The effect of nozzle arrangement and gas flow rate on mixing time
Jiang et al. 2019b	SKS furnace	Water model	Plume eye	A prediction equation for the size of the plume eye
Jiang et al. 2019a	A horizontal cylindrical vessel with side and bottom blow arrangement	Water model	Mixing behavior	The effect of horizontal distance between tuyeres, gas flow rate, and bath height on mixing time
Barron et al. 2010	A slice model of bottom blown P-S converter	CFD	Bubbling-jetting transition	The relation between gas flow rate and gas flow regime
Barron and Hernandez 2016	A slice model of side blown P-S converter	CFD	Bubbling-jetting transition	The relation between gas flow rate and gas flow regime
Zhao et al. 2018	A slice model of P-S converter with three tuyeres	Water model	Mass transfer and mixing behavior	The factors influencing mass transfer
Zhao et al. 2019a	A slice model of P-S converter with single tuyere	CFD	Mixing behavior	Velocity distribution, circular area, and wall shear stress at different operational parameters
Varmo et al. 1998	A slice model of P-S converter with two nozzles/tuyeres	Water model and CFD	Mixing behavior	Bubble characteristics
Almaraz et al. 2014	A slice model of P-S converter with one/three tuyeres	CFD	Mixing behavior with different tuyere number	The effect of tuyere number on mixing efficiency
Lio and Gray 1990	A slice model of P-S converter with three tuyeres	Water model	Transverse standing waves	Theoretical prediction of the period of a transverse standing wave
Chibwe et al. 2013	A slice model of P-S converter with single nozzle/tuyere	Water model and CFD	Mixing, mass transfer and phase distribution	The effect of gas flow rate and slag layer on mass transfer and phase distribution
Chibwe 2011	P-S converter	Water model and CFD	Mass transfer and mixing behavior	The effect of nozzle angle, gas flow rate, and bath height on mixing efficiency
Chibwe et al. 2015	P-S converter	Water model and CFD	Mixing behavior; an extra top lance	The effect of slag layer on mixing efficiency; encouraging results with combined top lance
Zhang et al. 2015	Vanyukov furnace	CFD	Mixing behavior	Phase distribution, velocity distribution, and the effect of gas flow rate on slag velocity
Valencia, Rosales-Vera and Orellana 2013	A slice model of Teniente furnace with one/two tuyeres	CFD	An extra tuyere at the bottom	Higher gas flow rate could be achieved by extra tuyeres at the bottom
Kapusta 2017	A common model for side blow arrangement	Water model	Gas jet penetration depth	The effect of gas flow regime on penetration depth
Akashi et al. 2020	TSL furnace	X-ray radioscopic visualization	Bubble behavior	Bubble characteristics
Zhao et al. 2016	TSL furnace	Water model	Mixing behavior	Higher efficiency with greater lance diameter and lance submerision depth
Zhao et al. 2019b	TSL furnace	Water model and CFD	Mixing behavior	The effect of turbulent viscosity and velocity vector on mixing time

interest to the industry, and no relevant reports were found.

- Due to the different physical properties between water and a high-temperature melt, the water model results of surface waves are not accurate enough to describe the wave behavior in the matte-slag system. CFD modeling work to describe the surface waves in copper making bath reactors is required.

Nomenclature

H_p [m]:	Penetration depth
D [m]:	Diameter of nozzle/tuyere/lance
Fr^* :	Modified Froude number
Re :	Reynold's number
ρ_g [kg·m ⁻³]:	Density of gas
ρ_l [kg·m ⁻³]:	Density of liquid
T_{mix} [s]:	Mixing time, evaluated by the diffusion time of tracers which usually indirectly measured by the change of electric resistance
H [m]:	Bath height
h [m]:	Lance submersion depth
Q [m ³ ·s ⁻¹]:	Volumetric gas flow rate
Ku :	Kutateladze number
U [m·s ⁻¹]:	Gas flow rate
σ [N·m ⁻¹]:	Liquid surface tension
g [m·s ⁻¹]:	Acceleration due to gravity
S_s [m]:	Simulated slag thickness
d_B [mm]:	Bubble diameter
θ [°]:	Angle between nozzle/tuyere and horizontal plane
A_{es} [m ²]:	The area of plume eye
H_l [m]:	Lower layer thickness
H_u [m]:	Upper layer thickness
U_p [m·s ⁻¹]:	Rising plume velocity
R_e [m]:	Equivalent radius
R [m]:	Vessel inner radius
α :	Dimensionless wave frequency
n :	The node of a specific wave ($n=1$ for 1 st asymmetric standing wave)
η :	The inner aspect ratio of model vessel
Q_{mL} [mL·s ⁻¹]:	Gas volumetric flow rate
θ_p [radian]:	The blowing angle between plume and vertical line
We :	Weber number

Disclosure statement

No potential conflict of interest was reported by the author(s).

Funding

This work was supported by the China Scholarship Council; School of Chemical engineering, Aalto university.

ORCID

Ari Jokilaakso  <http://orcid.org/0000-0003-0582-7181>

References

- Almaraz, A., C. López, I. Arellano, M. A. Barrón, D. Jaramillo, F. Reyes, and G. Plascencia. 2014. CFD modelling of fluid flow in a Peirce-Smith converter with more than one injection point. *Minerals Engineering* 56:102–08. doi:10.1016/j.mineng.2013.11.001.
- Asai, S., T. Okamoto, J. He, and I. Muchi. 1983. Mixing time of refining vessels stirred by gas injection. *Transactions of the Iron and Steel Institute of Japan* 23 (1):43–50. doi:10.2355/isijinternational1966.23.43.
- Baldock, B., K. Robilliard, J. Floyd, and B. Lightfoot. 1992. Top submerged lancing technology (Siros melt) for achieving difficult separations in smelting complex materials. *Mineral Processing and Extractive Metallurgy Review* 8 (1–4):245–26. doi:10.1080/08827509208952690.
- Ballal, N. B., and A. Ghosh. 1981. A water model study of bottom-blown oxygen steelmaking processes. *Metallurgical Transactions B* 12:525–34. doi:10.1007/BF02654323.
- Barron, M. A., C. Lopez, G. Plascencia, and I. Hilerio. 2010. Large eddy simulation of bubbling-jetting transition in a bottom blown copper converter. MSV 2010: proceedings of the 2010 international conference on modeling, simulation & visualization methods, 91–94. Las Vegas, NV.
- Barron, M. A., and C. A. Hernandez. 2016. Air-slag-matte interaction in a Peirce-Smith copper converter. Athens: The Steering Committee of The World Congress in Computer Science, Computer Engineering and Applied Computing (WorldComp), Las Vegas Nevada, USA.
- Bartos, P. J. 2002. SX-EW copper and the technology cycle. *Resources Policy* 28 (3–4):85–94. doi:10.1016/S0301-4207(03)00025-4.
- Bjurström, M., A. Tilliander, M. Iguchi, and P. Jönsson. 2006. Physical-modeling study of fluid flow and gas penetration in a side-blown AOD Converter. *ISIJ International* 46 (4):523–29. doi:10.2355/isijinternational.46.523.
- Brämning, M. 2010. Avoiding slopping in top-blown BOS vessels. Licentiate dissertation, 83. Luleå University of Technology.
- Brämning, M., G. Parker, S. Millman, A. Kapilashrami, D. Malmberg, and B. Björkman. 2011. Comparison between vessel vibration and audio-metry for slopping control in the Top-Blown BOS Process. *Steel Research International* 82:683–92. doi:10.1002/srin.201000275.
- Brimacombe, J. K., S. E. Meredith, and R. G. H. Lee. 1984. High-pressure injection of air into a Peirce-Smith copper converter. *Metallurgical Transactions B* 15:243–50. doi:10.1007/BF02667327.
- Cao, L. L., Q. Liu, Z. Wang, and N. Li. 2018. Interaction behaviour between top blown jet and molten steel during BOF steelmaking process. *Ironmaking & Steelmaking* 45 (3):239–48. doi:10.1080/03019233.2016.1255373.
- Chen, M., N. Wang, Y. Yao, J. Geng, and K. Xiong. 2007. Optimal mixing effect of LF Bottom-Blown stirring by two nozzles. *Steel Research International* 78:468–72. doi:10.1002/srin.200706233.
- Chibwe, D. K. 2011. *Flow behavior, mixing and mass transfer in a peirce-smith converter using physical model and computational fluid dynamics*. Stellenbosch University of Stellenbosch. University of Stellenbosch, South Africa.
- Chibwe, D. K., G. Akdogan, C. Aldrich, and P. Taskinen. 2013. Modelling of mixing, mass transfer and phase distribution in a Peirce-Smith converter model. *Canadian Metallurgical Quarterly* 52 (2):176–89. doi:10.1179/1879139512Y.0000000056.
- Chibwe, D. K., G. Akdogan, P. Taskinen, and J. J. Eksteen. 2015. Modelling of fluid flow phenomena in Peirce-Smith copper converters and analysis of combined blowing concept. *Journal of the South Africa Institute of Mining and Metallurgy* 115 (5):363–74. doi:10.17159/2411-9717/2015/v115n5a4.
- Coursol, P., P. J. Mackey, J. P. T. Kapusta, and N. C. Valencia. 2002. Energy consumption in copper smelting: A new asian horse in the race. *JOM* 67 (5):1066–74.
- Cui, Z., D. Shen, Z. Wang, W. Li, and R. Bian. 2010. New process of copper smelting with oxygen enriched bottom blowing technology. *Nonferrous Metals (Extractive Metallurgy)* 03:17–20. In Chinese.
- Devia, M., R. Parra, C. Queirolo, M. Sánchez, and I. Wilkomirsky. 2019. Copper smelting and converting: Past and present Chilean developments. *Mineral Processing and Extractive Metallurgy* 128 (1–2):108–16. doi:10.1080/25726641.2018.1542050.
- Elfsberg, J., and T. Matsushita. 2011. X-Ray observation of gas evolution, flotation, and emulsification of molten carbon steel immersed in mold flux. *Metallurgical and Materials Transactions B* 42:265–68. doi:10.1007/s11663-011-9475-8.
- Akashi, M., O. Keplinger, N. Shevchenko, S. Anders, M. Reuter, and S. Eckert. 2020. X-ray radioscopic visualization of bubbly flows injected through a top submerged lance into a liquid metal. *Metallurgical and Materials Transactions B* 51:124–39. doi:10.1007/s11663-019-01720-y.

- Ersso, M., A. Tilliander, M. Iguchi, L. Jonsson, and P. Jönsson. 2006. Fluid Flow in a Combined Top and Bottom Blown Reactor. *ISIJ International* 46 (8):1137–42. doi:10.2355/isijinternational.46.1137.
- Goto, M., E. Oshima, and M. Hayashi. 1998. Control aspects of the mitsubishi continuous process. *JOM* 50:60–64. doi:10.1007/s11837-998-0271-0.
- Guntoro, P. I., A. Jokilaakso, N. Hellstén, and P. Taskinen. 2018. Copper matte - slag reaction sequences and separation processes in matte smelting. *Journal of Mining and Metallurgy Section B: Metallurgy* 54 (3):301–11. doi:10.2298/JMMB180214021G.
- Guo, X., Q. Wang, Q. Tian, and B. Zhao. 2016. Analysis and optimization of oxygen bottom blowing copper smelting process. *Chinese Journal of Nonferrous Metals* 26 (3):689–98. In Chinese.
- Guo, X., Q. Wang, Q. Tian, and Y. Zhang. 2015. Non-steady multiphase equilibrium process of copper oxygen-enriched bottom blowing bath smelting with gradual change of oxygen and sulfur potential of different positions in furnace. *Chinese Journal of Nonferrous Metals* 25 (4):244–51. In Chinese.
- Habashi, F. 1995. The future of copper metallurgy. *Mineral Processing and Extractive Metallurgy Review* 15 (1–4):5–12. doi:10.1080/08827509508914178.
- He, C., N. Yang, Q. Huang, C. Liu, L. Wu, Y. Hu, Z. Fu, and Z. Gao. 2011. A Multi-Phase numerical simulation of a Four-Nozzle oxygen lance Top-Blown converter. *Procedia Earth and Planetary Science* 2:64–69. doi:10.1016/j.proeps.2011.09.011.
- Iguchi, M., K. Nakamura, and R. Tsujino. 1998. Mixing time and fluid flow phenomena in liquids of varying kinematic viscosities agitated by bottom gas injection. *Metallurgical and Materials Transactions B* 29:569–75. doi:10.1007/s11663-998-0091-1.
- Iguchi, M., S. Hosohara, T. Kondoh, Y. Itoh, and Z. Morita. 1993. Effect of the swirl motion of bubbling jet on the transport phenomena in a bottom blown bath. *ISIJ International* 79 (8):934–40.
- International Copper Study Group. 2019. The World Copper Factbook, *International Copper Study Group* 39.
- Jiang, X., Z. Cui, M. Chen, and B. Zhao. 2019a. Mixing behaviors in the horizontal bath smelting furnaces. *Metallurgical and Materials Transactions B* 50:173–80. doi:10.1007/s11663-018-1433-2.
- Jiang, X., Z. Cui, M. Chen, and B. Zhao. 2019b. Study of Plume Eye in the Copper Bottom Blown Smelting Furnace. *Metallurgical and Materials Transactions B* 50:782–89. doi:10.1007/s11663-019-01516-0.
- Kapusta, J. P. T. 2017. Submerged gas jet penetration: A study of bubbling versus jetting and side versus bottom blowing in copper bath smelting. *JOM* 69:970–79. doi:10.1007/s11837-017-2336-4.
- Kojo, I. V., A. Jokilaakso, and P. Hanniala. 2000. Flash smelting and converting furnaces: A 50 year retrospect. *JOM* 52 (2):57–61. doi:10.1007/s11837-000-0049-5.
- Kulkarni, A. A., and J. B. Joshi. 2005. Bubble formation and bubble rise velocity in gas-liquid systems a review. *Industrial & Engineering Chemistry Research* 44 (16):5873–931. doi:10.1021/ie049131p.
- Lai, Z., Z. Xie, and L. Zhong. 2008. Influence of bottom tuyere configuration on bath stirring in a top and bottom combined blown converter. *ISIJ International* 48 (6):793–98. doi:10.2355/isijinternational.48.793.
- Li, W. 2009. Ausmelt technology-developments in copper converting. *China Nonferrous Metallurgy* 1:1–5. In Chinese.
- Liow, J., and N. B. Gray. 1990. Slopping resulting from gas injection in a peirce-smith converter: Water modeling. *Metallurgical Transactions B* 21:987–96. doi:10.1007/BF02670269.
- Liu, Z., and L. Xia. 2019. The practice of copper matte converting in china. *Mineral Processing and Extractive Metallurgy* 128 (1–2):117–24. doi:10.1080/25726641.2018.1543147.
- Ma, J., P. Zhou, W. Cheng, Y. Song, and P. Shi. 2016. Dimensional analysis and experimental study of gas penetration depth model for submerged side-blown equipment. *Experimental Thermal and Fluid Science* 75:220–27. doi:10.1016/j.expthermflusci.2016.01.017.
- Mackey, P. J. 1982. The physical chemistry of copper smelting slags—a review. *Canadian Metallurgical Quarterly* 21 (3):221–60. doi:10.1179/cm.1982.21.3.221.
- Mackey, P. J., and R. Campos. 2001. Modern continuous smelting and converting by bath smelting technology. *Canadian Metallurgical Quarterly* 40 (3):355–76. doi:10.1179/cm.2001.40.3.355.
- Matousek, J. W. 1993. Oxygen potentials of copper smelting slags. *Canadian Metallurgical Quarterly* 32 (2):97–101. doi:10.1179/cm.1993.32.2.97.
- Matusewicz, R. W., M. A. Reuter, and S. P. Hughes. 2010. Large scale copper smelting using Ausmelt TSL technology at the Tongling Jinchang smelter. *Proceedings of Copper 2010*:961–70.
- Mazumdar, D., and R. I. L. Guthrie. 1986. Mixing models for gas stirred metallurgical reactors. *Metallurgical Transactions B* 17:725–33. doi:10.1007/BF02657134.
- Moskalyk, R. R., and A. M. Alfantazi. 2003. Review of copper pyrometallurgical practice: Today and tomorrow. *Minerals Engineering* 16 (10):893–919. doi:10.1016/j.mineng.2003.08.002.
- Newcomb, R. 1985. Shifting patterns of supply and demand in the world copper industry. *Mineral Processing and Extractive Metallurgy Review* 2 (1–2):1–20. doi:10.1080/08827508508952599.
- Nordquist, A., N. Kumbhat, L. Jonsson, and P. Jönsson. 2006. The effect of nozzle diameter, lance height and flow rate on penetration depth in a Top-blown water model. *Steel Research International* 77:82–90. doi:10.1002/srin.200606358.
- Prasad, M. S., V. P. Kenyen, and D. N. Assar. 1992. Development of SX-EW process for copper recovery—an overview. *Mineral Processing and Extractive Metallurgy Review* 8 (1–4):95–118. doi:10.1080/08827509208952680.
- Qu, S., T. Li, Z. Dong, and H. Luan. 2012. Discussion on production practice of oxygen-enriched bottom-blown smelting and design improvement of bottom-blown furnace. *China Nonferrous Metallurgy* 41 (1):10–13. In chinese.
- Robilliard, K. R., W. E. Short, G. A. Guorgi, and B. R. Baldock. 1994. Ausmelt's top submerged lance technology applied to copper smelting. In *Mining Latin America/Mineria Latinoamericana*, 411–21. Dordrecht: Springer.
- Rosales, M., R. Fuentes, P. Ruz, and J. Godoy. 1999. Fluid dynamic simulation of a teniente converter. In: *Proc. 4th Intl. conf. Copper 99-Cobre 99*, vol. 4, 107–21. USA: TMS.
- Rosales, M., P. Ruz, and R. Fuentes. 2003. Proceedings of the copper 2003-Cobre 2003, Hermann Schwarze Symposium. vol. 4, 485–98. Santiago, Chile: Canadian Institute of Mining, Metallurgy and Petroleum.
- Shao, P., and L. Jiang. 2019. Flow and mixing behavior in a new bottom blown copper smelting furnace. *International Journal of Molecular Science* 20:5757. doi:10.3390/ijms20225757.
- Shui, L., X. Ma, Z. Cui, and B. Zhao. 2018b. An Investigation of the behavior of the surficial longitudinal wave in a Bottom-Blown copper smelting furnace. *JOM* 70:2119–27. doi:10.1007/s11837-018-3046-2.
- Shui, L., Z. Cui, X. Ma, M. A. Rhamdhani, A. Nguye, and B. Zhao. 2015. Mixing phenomena in a bottom blown copper smelter: A water model study. *Metallurgical and Materials Transactions B* 46:1218–25. doi:10.1007/s11663-015-0324-z.
- Shui, L., Z. Cui, X. Ma, M. A. Rhamdhani, A. Nguyen, and B. Zhao. 2016. Understanding of Bath Surface Wave in Bottom Blown Copper Smelting Furnace. *Metallurgical and Materials Transactions B* 47:135–44. doi:10.1007/s11663-015-0466-z.
- Shui, L., Z. Cui, X. Ma, X. Jiang, M. Chen, Y. Xiang, and B. Zhao. 2018a. A water model study on mixing behavior of the Two-Layered bath in bottom blown copper smelting furnace. *JOM* 70:2065–70. doi:10.1007/s11837-018-2879-z.
- Southwick, L. M. 2008. William Peirce and E.A. Cappelen Smith and their amazing copper converting machine. *JOM* 60:24–34. doi:10.1007/s11837-008-0131-y.
- Stefanova, V., K. Genevski, and B. Stefanov. 2004. Mechanism of Oxidation of Pyrite, Chalcopyrite and Bornite During Flash Smelting. *Canadian Metallurgical Quarterly* 43 (1):78–88. doi:10.1179/cm.2004.43.1.78.
- Sundar, R., and R. B. H. Tan. 1999. A model for bubble-to-jet transition at a submerged orifice. *Chemical Engineering Science* 54 (18):4053–60. doi:10.1016/S0009-2509(99)00152-9.

- Svyatoslav, V. G., and N. Takashi. 2003. Wettability effect on bubble formation at nozzles in liquid aluminum. *Materials Transactions* 44 (11):2298–302. doi:10.2320/matertrans.44.2298.
- Tang, G., A. K. Silaen, H. Yan, Z. Cui, Z. Wang, H. Wang, K. Tang, P. Zhou, and C. Q. Zhou. 2017. CFD Study of Gas-Liquid Phase Interaction Inside a Submerged Lance Smelting Furnace for Copper Smelting. In *8th International Symposium on High-Temperature Metallurgical Processing*, 101–111. Cham: Springer.
- Tarassoff, P. 1984. Process R & D — The noranda process. *Metallurgical and Materials Transactions B* 15:411–32. doi:10.1007/BF02657372.
- Taskinen, P., A. Jokilaakso, D. Lindberg, and J. Xia. 2019b. Modelling copper smelting – The flash smelting plant, process and equipment. *Mineral Processing and Extractive Metallurgy* 128 (1–2):207–20.
- Taskinen, P., G. Akdogan, I. Kojo, M. Lahtinen, and A. Jokilaakso. 2019a. Matte converting in copper smelting. *Mineral Processing and Extractive Metallurgy* 128 (1–2):58–73. doi:10.1080/25726641.2018.1514774.
- Vaarno, J., J. Pitkälä, T. Ahokainen, and A. Jokilaakso. 1998. Modelling gas injection of a Peirce-Smith-converter. *Applied Mathematical Modelling* 22 (11):907–20. doi:10.1016/S0307-904X(98)10036-7.
- Vaisburd, S., A. Berner, D. G. Brandon, S. Kozhakhmetov, E. Kenzhaliyev, and R. Zhalev. 2002. Slags and mattes in Vanyukov's process for the extraction of copper. *Metallurgical and Materials Transactions B* 33 (4):551–59. doi:10.1007/s11663-002-0034-1.
- Valencia, A., M. Rosales-Vera, and C. Orellana. 2013. Fluid dynamics in a Teniente type copper converter model with one and two tuyeres. *Advances in Mechanical Engineering* 5. doi:10.1155/2013/902874.
- Wang, D., Y. Liu, Z. Zhang, P. Shao, and T. Zhang. 2013a. Experimental study of bottom blown oxygen copper smelting process for water model. *AIP Conference Proceedings* 1542:1304.
- Wang, D., Y. Liu, Z. Zhang, P. Shao, and T. Zhang. 2016. Dimensional Analysis of Average Diameter of Bubbles for Bottom Blown Oxygen Copper Furnace. *Mathematical Problems in Engineering* 2016. Article ID 4170371.
- Wang, D., Y. Liu, Z. Zhang, T. Zhang, and X. Li. 2017. PIV measurements on physical models of bottom blown oxygen copper smelting furnace. *Canadian Metallurgical Quarterly* 56 (5):1–11. doi:10.1080/00084433.2017.1310362.
- Wang, J., Y. Chen, W. Zhang, and C. Zhang. 2013b. Furnace structure analysis for copper flash continuous smelting based on numerical simulation. *Transactions of Nonferrous Metals Society of China* 23 (12):3799–807. doi:10.1016/S1003-6326(13)62932-5.
- Wang, Q., X. Guo, and Q. Tian. 2017d. Copper smelting mechanism in oxygen bottom-blown furnace. *Transactions of Nonferrous Metals Society of China* 27:946–53. doi:10.1016/S1003-6326(17)60110-9.
- Wang, Q., X. Guo, Q. Tian, M. Chen, and B. Zhao. 2017c. Reaction mechanism and distribution behavior of arsenic in the bottom blown copper smelting process. *Metals* 7:302. doi:10.3390/met7080302.
- Wang, Q., X. Guo, Q. Tian, T. Jiang, M. Chen, and B. Zhao. 2017a. Effects of matte grade on the distribution of minor elements (Pb, Zn, As, Sb, and Bi) in the bottom blown copper smelting process. *Metals* 7:502. doi:10.3390/met7110502.
- Wang, Q., X. Guo, S. Wang, L. Liao, and Q. Tian. 2017b. Multiphase equilibrium modeling of oxygen bottom-blown copper smelting process. *Transactions of Nonferrous Metals Society of China* 27 (11):2503–11. doi:10.1016/S1003-6326(17)60277-2.
- Wang, S., W. G. Davenport, S. Yao, A. Siegmund, T. Gonzales, G. Walters, and D. B. George. 2019. Copper Smelting: 2019 World Copper Smelter Data. In *Proc. of Copper 2019*, Vancouver August 18– 21. The Metallurgy and Materials Society of CIM, Canada.
- Wood, J., J. Hoang, and S. Hughes. 2017. Energy efficiency of the Outotec Ausmelt process for primary copper smelting. *JOM* 69 (6):1013–20. doi:10.1007/s11837-017-2322-x.
- Wood, J., S. Creedy, R. Matuszewicz, and M. Reuter. 2011. Secondary copper processing using Outotec Ausmelt TSL technology. In *Proceedings of Metplant*, 460–67. Carlton South: The Australasian Institute of Mining & Metallurgy.
- Yamashita, S., K. Miyamoto, M. Iguchi, and M. Zeze. 2003. Model Experiments on the mixing time in a bottom blown bath covered with top slag. *ISIJ International* 43 (11):1858–60. doi:10.2355/isijinternational.43.1858.
- Yazawa, A. 1974. Thermodynamic considerations of copper smelting. *Canadian Metallurgical Quarterly* 13 (3):443–53. doi:10.1179/cm.1974.13.3.443.
- Yazawa, A., and T. Azakami. 1969. Thermodynamics of removing impurities during copper smelting. *Canadian Metallurgical Quarterly* 8 (3):257–61. doi:10.1179/cm.1969.8.3.257.
- Yoshihiko, H., and T. Yukari. 2003. Effect of nozzle twisted lance on jet behavior and spitting rate in top blown process. *ISIJ International* 43 (9):1410–14. doi:10.2355/isijinternational.43.1410.
- Yu, Y., Z. Wen, X. Liu, G. Lou, F. Su, X. Hao, and Z. Lu. 2013. Study on Key Technology of Oxygen Enriched Bottom Blown Copper Melting Furnace. *The Chinese Journal of Nonferrous Metals* 4:12–16. In Chinese.
- Zhang, H., C. Zhou, W. Bing, and Y. Chen. 2015. Numerical simulation of multiphase flow in a Vanyukov furnace. *Journal of the South African Institute of Mining and Metallurgy* 115 (5):457–63. doi:10.17159/2411-9717/2015/v115n5a14.
- Zhang, Z., H. Yan, F. Liu, and J. Wang. 2013. Optimization analysis of lance structure parameters in oxygen enriched bottom-blown furnace. *The Chinese Journal of Nonferrous Metals* 23 (5):1471–78. In Chinese.
- Zhang, Z., Z. Chen, H. Yan, F. Liu, L. Liu, Z. Cui, and D. Shen. 2016. Numerical simulation of gas-liquid multi-phase flows in oxygen enriched bottom-blown furnace. *The Chinese Journal of Nonferrous Metals* 22 (6):1826–34. In Chinese.
- Zhao, H., P. Yin, L. Zhang, and S. Wang. 2016. Water model experiments of multiphase mixing in the top-blown smelting process of copper concentrate. *International Journal of Minerals Metallurgy and Materials* 23:1369–76. doi:10.1007/s12613-016-1360-7.
- Zhao, H., T. Lu, P. Yin, L. Mu, and F. Liu. 2019b. An experimental and simulated study on Gas-Liquid flow and mixing behavior in an ISASMELT furnace. *Metals* 9:565. doi:10.3390/met9050565.
- Zhao, H., X. Zhao, L. Mu, L. Zhang, and L. Yang. 2019a. Gas-liquid mass transfer and flow phenomena in a peirce-smith converter: A numerical model study. *International Journal of Minerals Metallurgy and Materials* 26:1092–104. doi:10.1007/s12613-019-1831-8.
- Zhao, X., H. Zhao, L. Zhang, and L. Yang. 2018. Gas-liquid mass transfer and flow phenomena in the Peirce-Smith converter: A water model study. *International Journal of Minerals Metallurgy and Materials* 25:37–44. doi:10.1007/s12613-018-1544-4.
- Zhou, X., M. Ersson, L. Zhong, and P. G. Jönsson. 2015. Numerical and physical simulations of a combined Top-Bottom-Side blown converter. *Steel Research International* 86:1328–38. doi:10.1002/srin.201400376.